

Gate-sensing coherent charge oscillations in a silicon field-effect transistor

Supplementary Information

M. Fernando Gonzalez-Zalba,^{*,†} Sergey N. Shevchenko,^{‡,¶,⊥} Sylvain Barraud,[§]
J.Robert Johansson,[¶] Andrew J. Ferguson,^{||} Franco Nori,^{¶,#} and Andreas C.
Betz[†]

*Hitachi Cambridge Laboratory, Cambridge, UK, B.Verkin Institute for Low Temperature
Physics and Engineering, Kharkov, Ukraine, Center for Emergent Matter Science, RIKEN,
Wako-shi, Saitama 351-0198, Japan, CEA/LETI-MINATEC, CEA-Grenoble, Grenoble,
France, and Cavendish Laboratory, University of Cambridge, UK*

E-mail: mg507@cam.ac.uk

*To whom correspondence should be addressed

[†]Hitachi Cambridge Laboratory, Cambridge, UK

[‡]B.Verkin Institute for Low Temperature Physics and Engineering, Kharkov, Ukraine

[¶]Center for Emergent Matter Science, RIKEN, Wako-shi, Saitama 351-0198, Japan

[§]CEA/LETI-MINATEC, CEA-Grenoble, Grenoble, France

^{||}Cavendish Laboratory, University of Cambridge, UK

[⊥]V. Karazin Kharkov National University, Kharkov, Ukraine

[#]Department of Physics, The University of Michigan, Ann Arbor, Michigan, USA

Differential Capacitance of a Double Quantum Dot

In the following section, we give a detailed calculation of the differential capacitance of a coupled double quantum dot probed by a single gate electrode (G) as depicted in Fig. S1a. The gate is coupled to the left and right dots via C_{GL} and C_{GR} respectively. The dots are coupled to ground via the source and drain tunnel barriers with capacitances C_{SL}, C_{DL} for the left dot and C_{SR}, C_{DR} for the right dot. The dots are tunnel coupled with mutual capacitance C_M .

Using the definition of differential capacitance,

$$C_{\text{diff}} = \frac{d(Q_L + Q_R)}{dV_G}, \quad (1)$$

the problem simplifies to calculating the sum of the gate polarization charge on the left (Q_L) and right dots (Q_R) as a function of gate voltage, V_G . This can be obtained knowing that the induced gate charges can be expressed as,

$$Q_L = C_{GL}(V_G - V_L) \quad (2)$$

$$Q_L = -e \langle n \rangle_L + (C_{SL} + C_{DL})V_L - C_M(V_R - V_L) \quad (3)$$

$$Q_R = C_{GR}(V_G - V_R) \quad (4)$$

$$Q_R = -e \langle n \rangle_R + (C_{SR} + C_{DR})V_R - C_M(V_L - V_R) \quad (5)$$

where $\langle n \rangle_{L(R)}$ and $V_{L(R)}$ are the average charge number and voltage on the left(right) island respectively. We solve this set of linear equations (2-5) to obtain the sum of induced charges,

$$Q_L + Q_R = \frac{1}{1 - \frac{C_M^2}{C_{\Sigma L} C_{\Sigma R}}} \{ [\alpha_L (C_{SL} + C_{DL}) + \alpha_R (C_{SR} + C_{DR})] V_G - e(\alpha_L \langle n \rangle_L + \alpha_R \langle n \rangle_R) + C_M \left[\left(\frac{\alpha_L}{C_{\Sigma R}} (C_{SL} + C_{DL}) + \frac{\alpha_R}{C_{\Sigma L}} (C_{SR} + C_{DR}) \right) V_G - \frac{e\alpha_L \langle n \rangle_R}{C_{\Sigma R}} - \frac{e\alpha_R \langle n \rangle_L}{C_{\Sigma L}} \right] \} \quad (6)$$

Here we have used the total capacitance of the dots $C_{\Sigma L(R)}$ and the correspondent lever arms $\alpha_{L(R)} = C_{GL(R)}/C_{\Sigma L(R)}$. If we consider the typical experimental situation in which $C_M \ll C_{\Sigma L(R)}$ and note that $\langle n \rangle_L = -\langle n \rangle_R$, for the situation in which dots exchange electrons, we find equation (2) in the main text,

$$C_{\text{diff}} = C_{\text{geom}} - e\alpha \frac{d \langle n \rangle_R}{dV_G} = C_{\text{geom}} + (e\alpha)^2 \frac{d \langle n \rangle_R}{d\varepsilon} \quad (7)$$

where $C_{\text{geom}} \approx \alpha_L (C_{SL} + C_{DL}) + \alpha_R (C_{SR} + C_{DR})$ and $\alpha \approx \alpha_R - \alpha_L$. Here we have used $\varepsilon = -\alpha(V_G - V_{G0})$ where V_{G0} stands for the value at which the energy levels exhibit an avoided crossing. The equivalent circuit diagram is depicted in Fig. S1b where we represent the capacitance parametric on V_G as $C_{\text{param}}(V_G)$

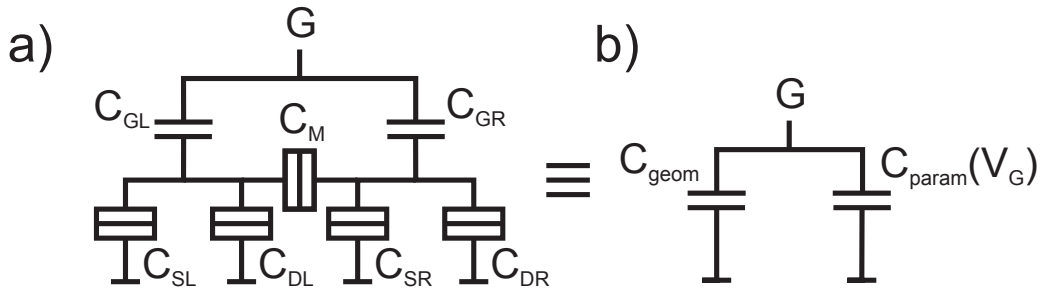


Fig. S 1: Double quantum dot capacitance circuit. DC (a) and AC equivalent circuits (b).

DC transport measurements

In Fig.2, we plot the source-drain DC current, I_{SD} , as function of the top gate voltage, V_G , and back-gate voltage, V_{BG} . The measurements are taken at 35 mK with a source drain voltage, $V_{SD}=1$ mV. At high V_G , we observe the transistor turning on and the exact gate voltage point at which this occurs depends upon the V_{BG} applied, decreasing for increasing V_{BG} . Close to the threshold voltage, we observe an oscillatory behaviour of the current characteristic of Coulomb blockade. This is due to the corner effect that confines electrons on to quantum dots at the top most corners of the transistor, as previously demonstrated.¹ In this voltage regime, the dots are well coupled to the source and drain allowing direct transport measurements to be taken.

A red square, superimposed on Fig. S2, indicates the region where the reflectometry measurements on the main text were taken. In this region, no direct transport through the transistor occurs as the dots are weakly coupled to the source and drain reservoir. This indicates that both dots are well centered in the channel along the transport direction and are not likely to be dopants diffused from the source and drain reservoir. However, the measurements in Fig. 1d of the main text reveal that reflectometry is a valuable tool for detecting charge motion where direct transport is not possible.

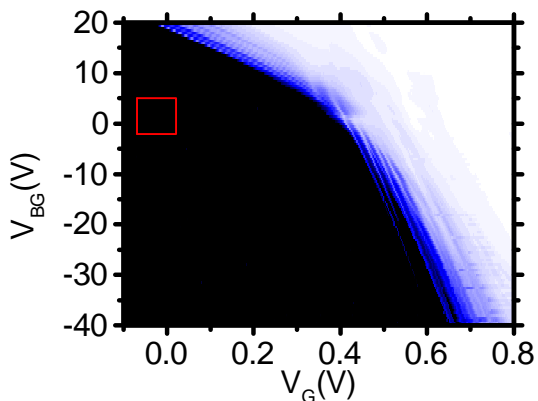


Fig. S 2: DC transport measurements. Source-drain current as a function of gate voltage and back-gate voltage at $V_{SD} = 1$ mV. The red square indicates the region where we perform reflectometry measurements in the main text.

Calibration of the microwave amplitude

We calibrated the microwave amplitude A_{mw} delivered to the double quantum dot using the following procedure. Initially, we calibrated the gate voltage axis V_G to energy detuning ε . In the LZS regime, interference fringes, as seen in Fig. 2b in the main text, appear at equidistant values of gate voltage given by the equation $\Delta V_G = hf_{\text{mw}}/e\alpha$ which provides a direct measurement of the gate coupling $\alpha=0.25$. Afterwards, we used the condition $A_{\text{mw}} = \varepsilon$, which delimits the voltage region in which LZS interference is observable, to calibrate the microwave generator output V_{mw} to microwave amplitude $A_{\text{mw}} = \kappa V_{\text{mw}}$. Here κ contains the attenuation of microwave line (including a total of -26 dB attenuators), PCB microwave stripline, sample's metallic pad and silicon channel. In Fig. S3, we plot the value of κ for several microwave frequencies. The frequency dependent attenuation of the line is well fitted by a $1/f_{\text{mw}}$ dependence, apart from the 34 GHz point which present a higher transmission. Hence we selected this frequency to perform most of the measurements in the main text.

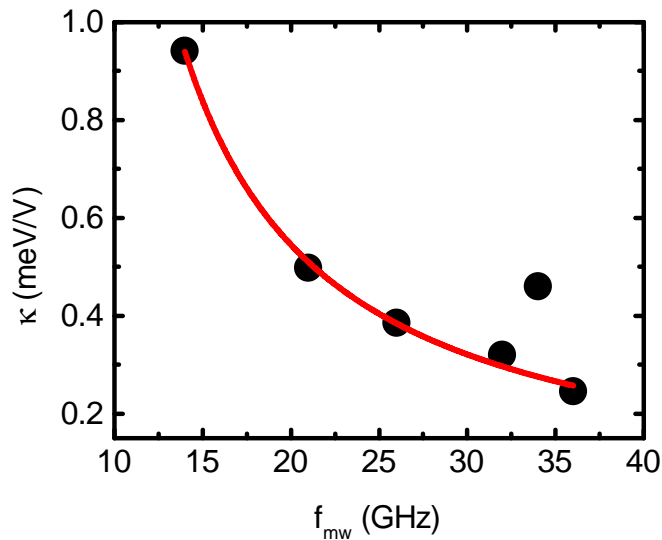


Fig. S 3: MW calibration. Microwave calibration factor κ as a function of frequency (black dots) and $1/f_{\text{mw}}$ fit (red solid line). The point at 34 GHz is not used for the fit.

Additionally, we performed measurements of the transmission of the microwave line at room temperature and obtained a total attenuation of -47 dB at 20 GHz, including -26 dB

attenuators and the on PCB launch stripline. These results allow us to estimate a \approx -9.5 dB attenuation of the sample’s source metallic pad and silicon channel.

Excited-state occupation probability

In this section, we present the calculated average excited state occupation probability P_1 used to calculate the resonator phase shift on the right panel of Fig. 3a in the main text. For the calculations we applied the formula from equation (7) in the main text using $T_2=T_1=100$ ps, $f_{mw}=34$ GHz and $\Delta_c=98 \mu\text{eV}$ as input parameters. In Fig. S4, we observe that the visibility in the qubit excited state probability is 60% since the average probability P_1 peaks at approximately 0.3.

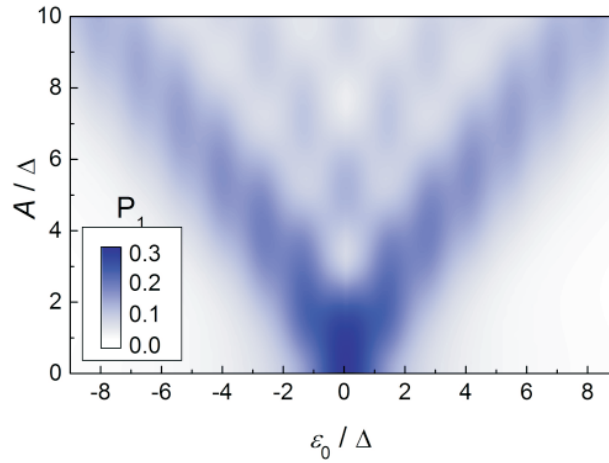


Fig. S 4: Excited state occupation probability P_1 as a function of reduced detuning ϵ_0/Δ and reduced microwave amplitude A/Δ . Here $\Delta=98 \mu\text{eV}$.

References

- (1) Voisin, B.; Nguyen, V.-H.; Renard, J.; Jehl, X.; Barraud, S.; Triozon, F.; Vinet, M.; Duchemin, I.; Niquet, Y.-M.; de Franceschi, S.; Sanquer, M. *Nano Letters* **2014**, *14*, 2094–2098.